

Resistivity model based on iFDS theory in $\text{Ga}_{1-x}\text{Mn}_x\text{As}$, $\text{La}_{1-x}\text{Ca}_x\text{MnO}_3$ and $\text{Mn}_x\text{Ge}_{1-x}$

Andrew Das Arulsamy¹

¹Condensed Matter Group, Division of Exotic Matter, No. 22, Jalan Melur 14, Taman Melur, 68000 Ampang, Selangor DE, Malaysia

(Dated: February 16, 2019)

Resistivity model in accordance with the ionization energy based Fermi Dirac statistics (iFDS) with further confinements from spin-disorder scattering is derived so as to capture the mechanism of both spin independent and spin-assisted charge transport in ferromagnets. The computed $T_{\text{crossover}}$ below T_C and carrier density in $\text{Ga}_{1-x}\text{Mn}_x\text{As}$ ($x = 6\text{-}7\%$) are 8-12 K and 10^{19} cm^{-3} , identical with the experimental values of 10-12 K and $10^{18}\text{-}10^{20} \text{ cm}^{-3}$ respectively. The calculated charge densities for $\text{Mn}_{0.02}\text{Ge}_{0.98}$ and $\text{La}_{1-x}\text{Ca}_x\text{MnO}_3$ ($x = 10\text{-}20\%$) are 10^{19} cm^{-3} and 10^{17} cm^{-3} respectively. We derive 1-dimensional iFDS wave functions for Dirac delta ($-\alpha\delta(x)$) and harmonic oscillator potentials ($m\omega^2x^2/2$). The iFDS ground state energy is shown to be consistent and exact with the ladder-operator and recursion-formula methods.

PACS numbers: 75.70.-i; 71.30.+h; 72.15.Rn; 75.50.Pp

Keywords: Ferromagnets, Fermi-Dirac statistics, Ionization energy, Resistivity model

I. INTRODUCTION

Diluted magnetic semiconductors (DMS) have tremendous potential for spintronics development and subsequently will lay the foundation to realize quantum computing. In order to exploit the spin assisted charge transport, one needs to understand the transport mechanism such as the variation of resistivity with temperature and doping in both paramagnetic and ferromagnetic phases. A wide variety of the magneto-electronic properties based on doping and Mn's valence state in manganites were reported to understand the transport mechanism(s).^{1,2} Furthermore, metallic conduction below T_C has been studied using double exchange mechanism (DEM) between *s* and *d* orbitals.³ Interestingly, Van Esch *et al.*⁴ have proposed multiple exchange interactions, which are ferromagnetic (FM) hole-hole and antiferromagnetic (AFM) Mn-hole interactions for DMS. These two effects, after neglecting the direct exchange between Mn-Mn (due to very diluted nature of DMS) are seem to be sufficient enough to describe the temperature dependent magnetization curves ($M(T)$) accurately. However, even after inclusion of FM and AFM effects including the spin disorder scattering, the transport property in the FM phase is still not well understood. Unfortunately, this is also true for the case of metallic property below T_C in the well known and extensively studied FM manganites as pointed out by Mahendiran *et al.*⁵ The resistivity ($\rho(T)$) above T_C for manganites is found to be in an activated form described by the equation,⁵

$$\rho(T > T_C) = \rho_0 \exp\left(\frac{E_a}{k_B T}\right). \quad (1)$$

E_a is the activation energy, ρ_0 and k_B denote the residual resistivity at $T \gg E_a$ and Boltzmann constant respectively. In the FM phase, the influence of $M(T)/M_0$ is

more pronounced than the electron-phonon (*e-ph*) contribution where the latter requires an overwhelmingly large coupling constant.⁵ Note that M_0 is the magnitude of magnetization at 0 K. Therefore, Mahendiran *et al.* have suggested that conventional mechanism namely, *e-ph* scattering has to be put aside so as to explain the $\rho(T)$ for manganites below T_C . On the contrary, $\rho(T)$ with *e-ph* involvement for DMS in the paramagnetic phase is given by⁴

$$\rho(T > T_C) = \frac{C_1 + C_2 [\exp(\Theta_D/T) - 1]^{-1}}{k_B T \ln [1 + \exp((E_m - E_f)/k_B T)]}. \quad (2)$$

The term, $C_2/[\exp(\Theta_D/T) - 1]$ takes care of the *e-ph* contribution. Θ_D , E_f , E_m , C_1 and C_2 represent the Debye temperature, Fermi level, mobility edge and numerical constants respectively. On the other hand, $\rho(T)$ in the FM phase based on the spin disorder scattering as derived by Tinbergen-Dekker is given by⁶

$$\begin{aligned} \rho_{SD}(T < T_C) = & \frac{(m_{e,h}^*)^{5/2} N(2E_F)^{1/2}}{\pi(n,p)e^2\hbar^4} J_{ex}^2 \\ & \times \left[S(S+1) - S^2 \left(\frac{M_{TD}(T)}{M_0} \right)^2 - S \left(\frac{M_{TD}(T)}{M_0} \right) \right. \\ & \left. \times \tanh \left(\frac{3T_C M_{TD}(T)}{2TS(S+1)M_0} \right) \right]. \end{aligned} \quad (3)$$

N is the concentration of nearest neighbor ions (Mn's concentration) while (n,p) is the concentration of charge carriers (electrons or holes respectively). $m_{e,h}^*$ denotes effective mass of electrons or holes, $\hbar = h/2\pi$, h = Planck constant. e is the charge of an electron, E_F and J_{ex} are the Fermi and FM exchange interaction energies respectively while S is the spin quantum number. Equation (3) becomes equivalent to Kasuya⁷ if one replaces the term,

$\tanh[3T_C M_{TD}(T)/2TS(S+1)M_0]$ with 1. Again, an accurate equation for the $\rho(T)$ below T_C is still lacking since spin disorder scattering alone is insufficient as shown by Tinbergen and Dekker⁶ as well as reviewed by Ohno.⁸

As a consequence, it is desirable to derive a formula that could describe the transport mechanism of ferromagnets for the whole temperature range i.e., for both paramagnetic and FM phases and even at very low T . With this in mind, the E_I based Fermi-Dirac statistics (iFDS) and spin disorder scattering based resistivity models will be employed in order to derive ρ as a function of T , E_I and $M_\rho(T, M_0)$. The consequences of $\rho(T, E_I, M_\rho(T, M_0))$ that arises from the variation of T , E_I and $M_\rho(T, M_0)$ are discussed in detail based on the experimental data reported by Van Esch *et al.*⁴, Mahendiran *et al.*⁵ and Park *et al.*⁹. The Mn_xGe_{1-x} FM semiconductor (FMS) is also accentuated here due to its promising properties for device applications⁹ where its gate voltage of ± 0.5 V is compatible with the present Complementary Metal-Oxide-Semiconductor (CMOS) and Ge's hole mobility ($110.68 \text{ m}^2\text{V}^{-1}\text{s}^{-1}$) is higher than GaAs ($12.65 \text{ m}^2\text{V}^{-1}\text{s}^{-1}$) and Si ($15.81 \text{ m}^2\text{V}^{-1}\text{s}^{-1}$). Mn_xGe_{1-x} 's resistivity is also semiconductor-like below T_C , which is more suitable than metallic $Ga_{1-x}Mn_xAs$. Moreover, Mn_xGe_{1-x} is also the simplest two-element system that can be utilized to evaluate the performance of the derived model consists of iFDS and $M_\alpha(T)$ (originates from τ_{SD}). $\alpha = K$ (calculated from the Kasuya's spin disorder scattering model), ρ (calculated from the resistivity model), \exp (determined experimentally).

II. RESISTIVITY MODEL BASED ON iFDS

The total current in semiconducting ferromagnets with contributions from both paramagnetic and FM phases is $J = \sum_\nu J_\nu$, $\nu = e^\downarrow, se^\uparrow, h^\downarrow, sh^\uparrow$. For convenience, the spin-up, \uparrow denotes the direction of the magnetic field or a particular direction below T_C , while the spin-down, \downarrow represents any other directions. Note that the total energy (Kinetic + Magnetic), $E_{K+M}^\uparrow \neq E_{K+M}^\downarrow$ due to energy level splitting below T_C . As such, the total current can be simplified as $J = J_e^\downarrow + J_{se}^\uparrow = J_e + J_{se}$ if the considered system is an *n*-type while $J = J_h + J_{sh}$ if it is a *p*-type. J_e and J_h are the spin independent charge current (electrons and holes respectively) in the paramagnetic phase whereas J_{se} and J_{sh} are the spin-assisted charge current in the FM phase. Thus the total resistivity (*n* or *p*-type) can be written as

$$\rho^{-1} = \rho_{e,h}^{-1} + \rho_{se,sh}^{-1} = \left[\frac{m_{e,h}^*}{(n,p)e^2\tau_e} \right]^{-1} + \left[\frac{m_{e,h}^*}{(n,p)e^2\tau_{SD}} \right]^{-1}. \quad (4)$$

τ_{SD} represents the spin disorder scattering rate. The carrier density for the electrons and holes (n, p) based on iFDS are given by^{10,11,12,13,16}

$$n = 2 \left[\frac{k_B T}{2\pi\hbar^2} \right]^{3/2} (m_e^*)^{3/2} \exp \left[\frac{E_F - E_I}{k_B T} \right]. \quad (5)$$

$$p = 2 \left[\frac{k_B T}{2\pi\hbar^2} \right]^{3/2} (m_h^*)^{3/2} \exp \left[\frac{-E_F - E_I}{k_B T} \right]. \quad (6)$$

iFDS is derived in a latter section in which, its applications are well documented in the Refs.^{10,11,12,13,14,15,16,17} Substituting $1/\tau_e = AT^2$ (due to electron-electron interaction), Eqs. (3) and (5) or (6) into Eq. (4), then one can arrive at

$$\rho_{e,se}(T) = \frac{AB \exp [(E_I + E_F)/k_B T]}{AT^{3/2}[M_\rho(T, M_0)]^{-1} + BT^{-1/2}}. \quad (7)$$

In which, $A = [A_{e,h}/2e^2(m_{e,h}^*)^{1/2}][2\pi\hbar^2/k_B]^{3/2}$, $B = 2m_{e,h}^* N(\pi E_F)^{1/2} J_{ex}^2/e^2\hbar k_B^{3/2}$ and $\tau_{SD}^{-1} = [N(2E_F)^{1/2}(m_{e,h}^*)^{3/2}/\pi\hbar^4] J_{ex}^2 M_\rho(T, M_0)$. $A_{e,h}$ is the T independent electron-electron scattering rate constant. Unlike band gap (E_g), $E_I + E_F$ in principle, is an electronic (charge related) gap. Conceptually, $E_I + E_F$ determines as to how an electron excites itself by overcoming the energy obstacles namely, E_I , $V(x)$ and E_g . In order to understand this, we will use the iFDS Hamiltonian in section IVD. The empirical function of the normalized magnetization is given by

$$M_\rho(T, M_0) = 1 - \frac{M_\rho(T)}{M_0}. \quad (8)$$

Equation (8) is an empirical function that directly quantifies the influence of spin alignments in the FM phase on the transport properties of charge and spin carriers in accordance with Eq. (7). In other words, the only way to obtain $\frac{M_\rho(T)}{M_0}$ is through Eq. (8). In fact, Eq. (8) is used to calculate $M_{TD}(T)/M_0$ and $M_K(T)/M_0$ by writing $S(S+1) - S^2\left(\frac{M_{TD}(T)}{M_0}\right)^2 - S\left(\frac{M_{TD}(T)}{M_0}\right) \tanh\left[\frac{3T_C M_{TD}(T)}{2TS(S+1)M_0}\right] = M_\rho(T, M_0)$ and $S(S+1) - S^2\left(\frac{M_K(T)}{M_0}\right)^2 - S\left(\frac{M_K(T)}{M_0}\right) = M_\rho(T, M_0)$ respectively. Consequently, one can actually compare and analyze the $M_\alpha(T)/M_0$ ($\alpha = TD, K, \rho$) calculated from Tinbergen-Dekker (TD), Kasuya (K) and Eq. (7) with the experimentally measured $M_{exp}(T)/M_0$. However, one has to switch to Eq. (9) given below for the hole-doped strongly correlated paramagnetic semiconductors, which is again based on iFDS.^{10,14}

$$\rho_h = \frac{A_h(m_h^*)^{-1}}{2e^2} \left[\frac{2\pi\hbar^2}{k_B} \right]^{3/2} T^{1/2} \exp \left[\frac{E_I + E_F}{k_B T} \right]. \quad (9)$$

A_h is the T independent electron-electron scattering rate constant. Equation (9) will be used to justify the

importance of the term J_{se} even if the resistivity is semiconductor-like in the FM phase. Note that, $m^* = m_e^* \approx m_h^* \approx (m_e^* m_h^*)^{1/2}$ is used for convenience. If however, $m_e^* \neq m_h^*$, then one just has to use the relation, $m^* = m_e^* m_h^* / (m_e^* + m_h^*)$. Even in the usual consideration for the total conductivity, $\sigma = \sigma_{electron} + \sigma_{hole}$, some algebraic rearrangements can lead one to the relation, $\rho(T) \propto \exp(E_I/k_B T) / [\exp(E_F/k_B T) + \exp(-E_F/k_B T)]$, exposing the consistent effect of E_I on transport properties.

III. DISCUSSION

A. Temperature-dependent resistivity curves

Resistivity versus temperature measurement ($\rho(T)$) is the most simplest and effective method to study the transport properties. In free-electron metals, the $\rho(T)$ curves are often exploited in order to deduce the T -dependence of the scattering rates namely, τ_{e-e} and τ_{e-ph} . Such behavior are well described by the Bloch-Grüneisen (BG) formula,¹⁸ given by

$$\rho_{BG} = \lambda_{tr} \frac{128\pi m^* k_B T^5}{ne^2 \Theta_D^4} \int_0^{\Theta_D/2T} \frac{x^5}{\sinh^2 x} dx. \quad (10)$$

λ_{tr} = electron-phonon coupling constant, n = free electrons concentration. The approximation of $\tau_{e-e}(T)$ and $\tau_{e-ph}(T)$ using Eq. (10) is valid basically because there are no other parameters that vary with T , apart from the said scattering rates. In fact, by utilizing the BG formula, one can reliably estimate that $\tau_{e-e}(T) \propto T^{-2}$ while $\tau_{e-ph}(T) \propto T^{-3 \rightarrow -5}$ for any experimentally viable Θ_D .

On the other hand, the metallic phenomenon observed in the ferromagnetic-metallic (FMM) phase below T_C in ferromagnets (FM) cannot be characterized as Fermi gas. Therefore, it is rather incorrect to extract $\tau_{e-e}(T)$, $\tau_{e-ph}(T)$ and $\tau_{magnons}(T)$ from the $\rho(T < T_C)$ curves in FM. Experimental evidences based on the photoemission, X-ray emission/absorption and extended X-ray emission fine structure spectroscopy have exposed the polaronic effect even at $T < T_C$ or in the FMM phase.¹⁹ Consequently, the charge density (n) in FMM phase is not T independent as one would anticipate for the free-electron metals (Fermi-gas). In addition, spin related mechanisms, like magnons and spin disorder scattering can be correctly represented with the normalized magnetization function, $M(T, M_0)$. It is quite common to employ Matthiessen's rule ($\tau^{-1} = \sum_i \tau_i^{-1}$) as opposed to the total current rule ($\tau = \sum_i \tau_i$) and write the resistivity below T_C in the form of

$$\rho(T) = \rho_0 + \sum_i A_i T^{\alpha_i}. \quad (11)$$

The i here indicates the types of T -dependent scattering rate that contribute to the resistivity and A is a T independent constant. ρ_0 is the T -independent scattering rate that originates from the impurities as $T \rightarrow 0$ K. The critical issue here is not about the validity of Matthiessen's rule, but on the validity of Eq. (11) in non free-electronic phase. Importantly, the T -dependent structure of Eq. (10) is equivalent to Eq. (11) that actually have enabled one to reliably calculate $\tau_{e-e}^{-1}(T)$ and $\tau_{e-ph}^{-1}(T)$ as $A_{e-e} T^2$ and $A_{e-ph} T^{3 \rightarrow 5}$ respectively. Equation (11) is extremely popular and it is applied indiscriminately to determine the T -dependence of a wide variety of scattering rates in FMM phase, while the correctness of such determination is still unclear and varies from one researcher to another.^{5,20,21} It is important to realize that only a free-electronic FMM phase at $T < T_C$ will justify the analysis based on Eq. (11). The influence of polaronic effect and magnetization function (the variation of $M(T)/M_0$ with T) reinforces the T -dependence of charge density, which point towards the inapplicability of Eq. (11) in FMM phase.

B. $\text{Ga}_{1-x}\text{Mn}_x\text{As}$

The resistivity measurements⁴ and its fittings based on Eqs. (7) and (9) are shown in Fig. 1 a) and b) respectively for $\text{Ga}_{1-x}\text{Mn}_x\text{As}$. One needs two fitting parameters (A and E_I) for $\rho(T > T_C)$ and another two (B and $M_\rho(T, M_0)$) for $\rho(T < T_C)$. All the fitting parameters are listed in Table I. Note that $S = 1$ and $5/2$ are employed for the fittings of $M_K(T)/M_0$ while T_C and $T_{crossover} = T_{cr}$ were determined from the experimental resistivity curves. The deviation of $M_K(T)/M_0$ from the M_{exp}/M_0 increases with S from $1 \rightarrow 5/2$. The $\rho(T)$ is found to increase with x from 0.060 to 0.070 due to the mechanism proposed by Van Esch *et al.*^{4,22} and Ando *et al.*²³ They proposed that neutral Mn^{3+} acceptors that contribute to magnetic properties could be compensated by As, where for a higher concentration of Mn, instead of replacing Ga it will form a six-fold coordinated centers with As (Mn^{6As}).^{4,22,23} These centers will eventually reduce the magnitude of ferromagnetism (FM) in DMS due to the loss of spin-spin interaction between $\text{Mn}(3d^5)$ and h . Equations. (7) and (9) also predict that if Mn^{2+} ($E_I = 1113 \text{ kJmol}^{-1}$) or Mn^{3+} ($E_I = 1825 \text{ kJmol}^{-1}$) substitutes Ga^{3+} ($E_I = 1840 \text{ kJmol}^{-1}$), then $\rho(T)$ should further decrease with x , which is not the case here. Thus, Mn^{2+} or Mn^{3+} do not substitute Ga^{3+} . Interestingly, the T_{crs} observed in $\text{Ga}_{0.940}\text{Mn}_{0.060}\text{As}$ (annealed: 370°C) and $\text{Ga}_{0.930}\text{Mn}_{0.070}\text{As}$ (as grown) are 10 K and 12 K, respectively, which are identical with the calculated values of 8 K and 12 K, respectively from Eq. (7). Note here that $E_I + E_F = T_{cr}$. The calculated carrier density using $E_I + E_F = 8 \text{ K}, 12 \text{ K}$, m_h^* = rest mass and Eq. (6) is $2.4 \times 10^{19} \text{ cm}^{-3}$. Below T_C , spin alignments enhance the contribution from J_{se} and reduces the exponential increase of $\rho(T)$. This reduction in $\rho(T)$ is as a

result of dominating J_{se} and the small magnitude of $E_I + E_F$ (8 K, 12 K). Consequently, exponential effect only comes at $T < 12$ K, as clearly shown in Fig. 1 a). The $\text{Ga}_{0.930}\text{Mn}_{0.070}\text{As}$ samples after annealing at 370 °C and 390 °C do not indicate any FM (Fig. 1 b)).⁴ Thus the fittings are carried out with Eq. (9) that only requires two fitting parameters namely, A and $E_I + E_F$ since $J_{se} = 0$ (there is no observable T_C) and/or $dM_\alpha(T)/M_0dT = 0$ ($M_\rho(T, M_0) = \text{constant}$). The exponential increase in Fig. 1 b) for $\rho(T)$ is due to $E_I + E_F$ from Eq. (9) with zilch J_{se} contribution.

Figure 1 c) and d) indicate the normalized magnetization, $M_\alpha(T)/M_0$. Note that $M_{\rho,TD,K}(T)/M_0$ is a fitting parameter that has been varied accordingly to fit $\rho(T < T_C)$. Equation (8) is used to calculate $M_{\rho,TD,K}(T)/M_0$ with $S = 1$. $M_{\rho,TD,K}(T)/M_0$ is also compared with the experimentally determined⁴ $M_{exp}(T)/M_0$ as depicted in Fig. 1 d). One can easily notice the inequality, $M_{TD}(T)/M_0 > M_K(T)/M_0 > M_\rho(T)/M_0 > M_{exp}(T)/M_0$ from Fig. 1 c) and d). As such, $M_\rho(T)/M_0$ from Eq. (7) is the best fit for the experimentally measured $M_{exp}(T)/M_0$. However, $M_\rho(T)/M_0$ is still larger than $M_{exp}(T)/M_0$, because resistivity measures only the path with relatively lowest E_I and with easily aligned spins that complies with the principle of least action. On the contrary, the magnetization measurement quantifies the average of all the spins' alignments.

C. $\text{La}_{1-x}\text{Ca}_x\text{MnO}_3$

Mahendiran *et al.*⁵ discussed $\rho(T < T_C)$ with respect to Eq. (1) and obtained the activation energy, $E_a = 0.16$ eV for $x = 0.1$ and 0.2 of $\text{La}_{1-x}\text{Ca}_x\text{MnO}_3$ samples at 0 T. Using Eq. (7) however, $E_I + E_F$ for $x = 0.1$ and 0.2 samples are calculated to be 0.12 and 0.11 eV respectively. The calculated carrier density using $E_I + E_F = 0.12$ eV, 0.11 eV, $m_h^* = \text{rest mass}$ and Eq. (6) gives 10^{17} cm⁻³. In the presence of $\mathbf{H} = 6$ T, $E_I + E_F = 0.0776$ eV for $x = 0.2$ and $p = 10^{18}$ cm⁻³. It is proposed that the activated behavior for $\rho(T > T_C)$ is due to E_I .¹⁰ The fittings are shown in Fig. 2 a) and b) while its fitting parameters are listed in Table I. Theoretically,¹⁰ Ca²⁺ ($E_I = 868$ kJmol⁻¹) < La³⁺ ($E_I = 1152$ kJmol⁻¹), therefore $\rho(T)$ is expected to decrease with Ca²⁺ doping significantly. On the contrary, only a small drop in $E_I + E_F$ is observed between $x = 0.1$ (0.12 eV) and 0.2 (0.11 eV) and this is due to Mn⁴⁺'s compensation effect. In other words, the quantity of Mn⁴⁺ increased with x . In fact, the quantity of Mn⁴⁺ increased 6% from $x = 0.1$ (19%) to 0.2 (25%).⁵ Ideally, the difference in E_I between Ca²⁺ and La³⁺ is $1152 - 868 = 284$ kJmol⁻¹. But, due to compensation with 6% Mn^{3+→4+} ($E_I = 4940$ kJmol⁻¹: 4th ionization energy), the actual difference is only $284 - [75\%(1825) + 25\%(4940) - 81\%(1825) - 19\%(4940)] = 97$ kJmol⁻¹. 1825 kJmol⁻¹ is the E_I for Mn³⁺. This calculation simply exposes the compensation effect in which,

6% of Mn⁴⁺ reduces the Ca²⁺ effect from 284 kJmol⁻¹ to 97 kJmol⁻¹.

At 6 T, $\text{La}_{0.8}\text{Ca}_{0.2}\text{MnO}_3$ indicates a much lower resistivity (Fig. 2 b)). The result that larger \mathbf{H} giving rise to overall conductivity is due to large amount of aligned spins that gives rise to J_{se} . Hence, $E_I + E_F$ at 6 T (78 meV) is less than $E_I + E_F$ at 0 T (112 meV). Figure 2 c) and d) depict the calculated $M_\alpha(T)/M_0$ with $S = 1$ and $M_{exp}(T)/M_0$ for $x = 0.2$ respectively. The calculated $M_{TD}(T)/M_0$ is dropped for $\text{La}_{1-x}\text{Ca}_x\text{MnO}_3$ since $M_K(T)/M_0$ seems to be a better approximation than $M_{TD}(T)/M_0$ as indicated in Fig. 1 c) and d). The discrepancy between $M_\rho(T)/M_0$ and $M_{exp}(T)/M_0$ still exists even though Eq. (7) reproduces $\rho(T)$ at all T range accurately. Again, this discrepancy is due to the principle of least action as stated earlier. In addition, the manganites' charge transport mechanism below T_C is also in accordance with Eq. (7) because the term, $M_\rho(T, M_0)$ handles the exchange interactions' complexities separately for DMS and manganites. For example, one can clearly notice the different type of discrepancies between DMS and manganites by comparing the empirical function, $M_\alpha(T)/M_0$ ($\alpha = \rho, \text{exp}$) between Fig. 1 d) and Fig. 2 d). Hence, Eq. (7) is suitable for both types of ferromagnets, be it diluted or concentrated.

D. $\text{Mn}_x\text{Ge}_{1-x}$

The $\text{Mn}_x\text{Ge}_{1-x}$ FMS with homogeneous Mn concentration has been grown using low- T MBE technique.⁹ The $\text{Mn}_x\text{Ge}_{1-x}$ was found to be a *p*-type with carrier density in the order of $10^{19} - 10^{20}$ cm⁻³ for $0.006 \leq x \leq 0.035$ as measured by Park *et al.*⁹ Both the resistivity measurements⁹ and its fittings based on Eq. (7) are shown in Fig. 3 a). Here, $E_I + E_F$, A and B have been floated while $M_\rho(T, M_0)$ is constrained to reduce with T in order to fit the experimental $\rho(T, x = 0.02)$. The absence of the Curie-Weiss law in the $\rho(T, x = 0.02)$ curve is due to insufficient number of aligned spins that eventually leads to a relatively small J_{se} , which in turn, is not able to produce the metallic conduction below T_C . This scenario is also in accordance with the measured $M_{exp}(T)$ where, only 1.4-1.9 μ_B/Mn atom contributes to ferromagnetism as compared with the ideal value of 3.0 μ_B/Mn atom. In other words, only 45-60% of Mn ions are magnetically active.⁹ It is found that $E_I + E_F = 15$ K from the $\rho(T)$ fitting for $\text{Mn}_{0.02}\text{Ge}_{0.98}$. Subsequently, one will be able to calculate the hole concentration as 2.38×10^{19} cm⁻³ using Eq. (6) and $m_h^* = \text{rest mass}$, which is remarkably in the vicinity of the experimental value,⁹ $10^{19} - 10^{20}$ cm⁻³. Interestingly, the semiconductor-like behavior of $\rho(T, x = 0.02)$ below T_C is *not* exponentially driven as the value of $E_I + E_F$ is very small (15 K) to be able to contribute significantly above 15 K. Rather, it is the T -dependence of Eq. (7) determines $\rho(T, x = 0.02)$ below T_C . Add to that, we also found Eq. (9) could not represent the experimental $\rho(T, x = 0.02)$ as shown

in Fig. 3 a) with $A_h = 1.8$, $E_I + E_F = 80$ K and $p = 1.92 \times 10^{19} \text{ cm}^{-3}$. It seems that, in the absence of J_{se} term, Eq. (9) is inadequate to capture the T -dependence of $\rho(T, x = 0.02)$ in the FM phase, which justifies the non-exponential behavior.

The pronounced effect of Eq. (8) can be noticed by comparing the calculated plots between Eq. (7) and Eq. (7) with additional constraint, $dM_\rho(T)/dT = 0$ as indicated in Fig. 3 a). Recall that Eq. (8) is varied with T to fit the experimental $\rho(T, x = 0.02)$ in compliance with Eq. (7). Furthermore, $\rho(T)$ is found⁹ to decrease with x from 0.016 to 0.02 while $\rho(T, x = 0.02)$ remains identical with $\rho(T, x = 0.033)$. This type of transition can be readily evaluated with Eq. (7). Firstly, notice the large increase in room temperature p from 10^{14} cm^{-3} (upper limit) for pure Ge to 10^{19} cm^{-3} (lower limit) for a mere 2% Mn substituted $\text{Mn}_{0.02}\text{Ge}_{0.98}$, which gives rise to a rapid decrease of $\rho(T, x)$. The average E_I s for Mn^{2+} , Mn^{3+} and Ge^{4+} are computed as 1113, 1825 and 2503 kJmol^{-1} respectively. According to iFDS, Mn substitution into Ge sites will reduce the magnitude of $\rho(T)$ since $E_I(\text{Ge}^{4+}) > E_I(\text{Mn}^{3+}) > E_I(\text{Mn}^{2+})$, regardless whether $dM(T)/dT = 0$ or $dM(T)/dT \neq 0$. Such behavior has been observed experimentally⁹ where, $\rho(T, x = 0.009) > \rho(T, x = 0.016) > \rho(T, x = 0.02)$. Surprisingly however, $\rho(T, x = 0.02) \simeq \rho(T, x = 0.033)$. On the contrary, using iFDS, one should get $\rho(T, x = 0.02) > \rho(T, x = 0.033)$. If $\rho(T, x = 0.02) \simeq \rho(T, x = 0.033)$, then $\text{Mn}^{2+,3+}$ ($0.033 - 0.02 = 0.013$) may not have substituted Ge, instead it could have formed a well segregated impurity phase and/or Mn^{4+} concentration have increased with x . Notice that the formation of impurity phase is quite common in any system, including $\text{Ga}_{1-x}\text{Mn}_x\text{As}$ DMS with strictly limited Mn solubility. The normalized magnetization, $M_{K,\rho,\text{exp}}(T)/M_0$ for $\text{Mn}_{0.02}\text{Ge}_{0.98}$ have been plotted in Fig. 3 b). One can notice the relation, $M_K(T)/M_0 > M_\rho(T)/M_0 > M_{\text{exp}}(T)/M_0$ from Fig. 3 b). Again, $M_\rho(T)/M_0 > M_{\text{exp}}(T)/M_0$ is due to the ability of both J_e and J_{se} to follow the easiest path. Additionally, the T -dependence of $M_{\text{exp}}(T)$ is similar to $\text{Ga}_{1-x}\text{Mn}_x\text{As}$ rather than the well established manganite ferromagnets, which reveals the possibility of multiple exchange interactions^{4,9,22}. All the values of E_I discussed above were averaged in accordance with $E_I[X^{z+}] = \sum_{i=1}^z \frac{E_{Ii}}{z}$. Prior to averaging, the 1st, 2nd, 3rd and 4th ionization energies for all the elements mentioned above were taken from Ref.²⁴

IV. iFDS THEORY

A. iFDS Hamiltonian and zero potential

We consider the free-particle Hamiltonian of mass m moving in 1-dimension of an infinite square well (width = a), which is given by (after making use of the linear momentum operator, $\hat{\mathbf{p}} = -i\hbar\partial/\partial x^2$).

$$\hat{H} = \frac{\hat{p}^2}{2m} = -\frac{\hbar^2}{2m} \frac{\partial^2}{\partial x^2}. \quad (12)$$

Subsequently, one can write the time-independent Schrödinger equation for the same particle, however in an unknown potential, $V(x)$ as

$$\begin{aligned} -\frac{\hbar^2}{2m} \frac{\partial^2 \varphi}{\partial x^2} &= (E + V(x))\varphi \\ &= (E_0 \pm \xi)\varphi. \end{aligned} \quad (13)$$

In the second line of Eq. (13), one can notice that the influence of the potential energy on the total energy of that particular particle has been conveniently parameterized as $E_0 \pm \xi$ and this is not an approximation. In fact, we will show this in the sections to come by calculating the bound and ground state energies for $V(x) = -\alpha\delta(x)$ and $V(x) = \omega^2 x^2/2$, respectively. The energy function, ξ will be characterized later in such a way that one can replace $E + V(x)$ with $E_0 \pm \xi$ in which, $E_0 = E$ at $T = 0$. We rewrite Eq. (13) to get

$$\frac{\partial^2 \varphi}{\partial x^2} = -\frac{2m}{\hbar^2} [E_0 \pm \xi]\varphi \quad (14)$$

and

$$\frac{\hbar^2 k^2}{2m} = E_0 \pm \xi = \frac{\hbar^2}{2m} [k_0^2 \pm k_\xi^2]. \quad (15)$$

$k^2 = (2m/\hbar^2)[E_0 \pm \xi]$. E and E_0 in a given system range from $+\infty$ to 0 for electrons and 0 to $-\infty$ for holes that eventually explains the \pm sign in ξ . Now, Eq. (13) can be solved to give

$$\varphi_n = C \sin[(k_0^2 \pm k_\xi^2)^{1/2} x]. \quad (16)$$

After normalization, $\int_0^a |C|^2 \sin^2[(k_0^2 \pm k_\xi^2)^{1/2} x] dx = |C|^2 a/2 = 1$, one obtains $C = \sqrt{2/a}$. Finally, the normalized wave function,

$$\varphi_n = \sqrt{\frac{2}{a}} \sin[(k_0^2 \pm k_\xi^2)^{1/2} x]. \quad (17)$$

Applying the boundary conditions for free-electrons, $V(x) = 0$; $\xi = E - E_0 + [V(x) = 0] = E - E_0$; $E = E_0 \pm \xi$, $\varphi(0) = 0$ and $\varphi(a) = 0$ require $(k_0^2 \pm k_\xi^2)^{1/2} = n\pi/a$. Eventually, one arrives at

$$\varphi_n = \sqrt{\frac{2}{a}} \sin\left[\frac{n\pi}{a} x\right]. \quad (18)$$

Obviously, one can also obtain the exact form of Eq. (18) from the 1D time-independent Schrödinger equation with $V(x) = 0$ and $k_n = n\pi/a$.²⁵

B. Dirac delta potential

There can be many general solutions for Eq. (13) with $V(x) \neq 0$ and these solutions can be derived in such a way that they can be compared, term by term with known wave functions. For example, If $V(x) = -\alpha\delta(x)$, then we need a solution in the form of $\varphi(x) = C \exp[-i\alpha x]$ and the associated iFDS wave function can be derived as

$$\frac{\partial \varphi(x)}{\partial x} = -iaC \exp[-i\alpha x].$$

$$\frac{\partial^2 \varphi(x)}{\partial x^2} = -a^2 \varphi(x).$$

Using Eq. (14), we find

$$a = \left[\frac{2m}{\hbar^2} (E_0 \pm \xi) \right]^{1/2}.$$

Therefore,

$$\varphi(x) = C \exp[-i(k_0^2 \pm k_\xi^2)^{1/2} x]. \quad (19)$$

Normalizing φ gives

$$1 = \int_{-\infty}^{+\infty} |\varphi(x)|^2 dx = 2|C|^2 \int_0^{+\infty} e^{-2i(k_0^2 \pm k_\xi^2)^{1/2} x} dx \\ = \frac{C^2}{i(k_0^2 \pm k_\xi^2)^{1/2}}. \quad (20)$$

Consequently,

$$\varphi(x) = i^{1/2} [k_0^2 \pm k_\xi^2]^{1/4} \exp[-i(k_0^2 \pm k_\xi^2)^{1/2} x]. \quad (21)$$

Term by term comparison between Eq. (21) and²⁵

$$\varphi(x) = \frac{m\alpha}{\hbar} \exp\left[-\frac{m\alpha|x|}{\hbar^2}\right],$$

gives the bound state energy, $E_0 \pm \xi = -m\alpha^2/2\hbar^2$ after making use of Eq. (15) and $[i^2(k_0^2 \pm k_\xi^2)]^{1/4} = m\alpha/\hbar$ or $-i(k_0^2 \pm k_\xi^2)^{1/2} x = -m\alpha|x|/\hbar^2$.

C. Harmonic oscillator potential

Another example is the 1D harmonic oscillator and now we need a solution in the form of $\varphi(x) = C \exp[-ax^2]$ of which, the corresponding normalized iFDS wave function can be derived as

$$\ln \varphi(x) = \ln C - ax^2 \ln e.$$

$$\frac{1}{\varphi(x)} \frac{\partial \varphi(x)}{\partial x} = -2ax.$$

$$\frac{\partial^2 \varphi(x)}{\partial x^2} = 2a\varphi(x)[2ax^2 - 1].$$

Again, using Eq. (14) we find,

$$a = \frac{1}{2}(k_0^2 \pm k_\xi^2).$$

Normalizing φ gives

$$1 = \int_{-\infty}^{+\infty} |\varphi(x)|^2 dx = 2|C|^2 \int_0^{+\infty} e^{-2ax^2} dx \\ = 2|C|^2 \frac{1}{2} \left[\frac{\pi}{2a} \right]^{1/2}$$

and

$$C = \left[\frac{k_0^2 \pm k_\xi^2}{\pi} \right]^{1/4}.$$

Consequently,

$$\varphi(x) = \left[\frac{(k_0^2 \pm k_\xi^2)}{\pi} \right]^{1/4} \exp\left[-\frac{1}{2}(k_0^2 \pm k_\xi^2)x^2\right]. \quad (22)$$

The corresponding Schrodinger equation is given by

$$-\frac{\hbar^2}{2m} \frac{\partial^2 \varphi}{\partial x^2} = \left[\frac{2m}{\hbar^2} (E_0 \pm \xi)^2 x^2 - (E_0 \pm \xi) \right] \varphi. \quad (23)$$

Again, we compare Eq. (22) with,²⁵

$$\varphi_0(x) = \left[\frac{m\omega}{\pi\hbar} \right]^{1/4} \exp\left[-\frac{m\omega}{2\hbar} x^2\right]. \quad (24)$$

In doing so, we can show that the ground state energy, $E_0 \pm \xi = \frac{1}{2}\hbar\omega$ either from $[m\omega/\pi\hbar]^{1/4} = [(k_0^2 \pm k_\xi^2)/\pi]^{1/4}$ or $-(k_0^2 \pm k_\xi^2)x^2/2 = -mx^2\omega/2\hbar$. In summary, we have established the iFDS method by calculating the first bound and ground state energies as given in Eqs. (21) and (22). In addition, Eq. (22) is consistent with the wave functions derived from the ladder-operator and recursion-formula methods. As such, we can build on

Eq. (22) to obtain the energy at the n th state. In particular, the total energy at the n th state is given by $(E_0 \pm \xi)_n = (2n+1)(E_0 \pm \xi)$ after utilizing the relation, $E_n = (n+1/2)\hbar\omega$. The *iFDS* wave function at the n th state can be derived by using the Hermite polynomials ($H_n(\zeta)$) based wave function, derived from the recursion formula as given below²⁵

$$\varphi_n(x) = \left[\frac{m\omega}{\pi\hbar} \right]^{1/4} \frac{1}{2^n n!} H_n(\zeta) \exp \left[-\frac{m\omega}{2\hbar} x^2 \right].$$

Where, $\zeta = (m\omega/\hbar)^{1/2}x$. Using Eqs. (22) and (24), we find

$$\frac{m\omega}{\hbar} = k_0^2 \pm k_\xi^2.$$

Hence,

$$\zeta_{iFDS} = x [k_0^2 \pm k_\xi^2]^{1/2}.$$

Finally, the *iFDS* wave function at the n th state can be shown as

$$\begin{aligned} \varphi_n(x) &= \left[\frac{(k_0^2 \pm k_\xi^2)}{\pi} \right]^{1/4} \frac{1}{2^n n!} H_n(\zeta_{iFDS}) \\ &\times \exp \left[-\frac{1}{2}(k_0^2 \pm k_\xi^2)x^2 \right]. \end{aligned}$$

D. Ionization energy in *iFDS*

From Eq. (13), it is obvious that the magnitude of ξ is given by $\pm\xi = E - E_0 + V(x)$ and this is exactly the energy needed for a particle to overcome the bound state and the potential that surrounds it. Therefore, we apply the concept of ionization energy where, $\xi = E_I^{real} = E_I + V(x)$ or $\xi = E_I + [V(x) = 0] = E_I$, to justify that an electron to occupy a higher state N from initial state M is more probable than from initial state L if the condition $E_I(M) < E_I(L)$ at certain T is satisfied. As for a hole to occupy a lower state M from initial state N is more probable than to occupy state L if the same condition above is satisfied. Now, it is clear that the total energy, $E = E_0 \pm \xi = E_0 \pm E_I$ for $V(x) = 0$ (Fermi gas: infinite square well potential) and $E = E_0 \pm \xi = E_0 \pm E_I^{real}$ for $V(x) \neq 0$ in harmonic oscillator and Dirac delta potentials. We further justify the E_I concept in *iFDS* distribution function derived in the next section. The exact E_I values are known for an isolated atom. In this case, E_I can be evaluated with

$$E_I = \sum_i^z \frac{E_{Ii}}{z}. \quad (25)$$

However, substituting the same atom in a crystal gives rise to the influence of $V(x)$ and in reality, E_I^{real} cannot be evaluated from Eq. (25). Nevertheless, the E_I^{real} of an atom or ion in a crystal is proportional to the isolated atom and/or ion's E_I as written below.

$$\begin{aligned} E_I^{real} &= \alpha \sum_i^z \frac{E_{Ii}}{z} \\ &= \alpha E_I. \end{aligned} \quad (26)$$

The $i = 1, 2, \dots, z$ represent the first, second,... ionization energies in which, z is the oxidation number of a particular ion. E_I^{real} is actually equal to the energy needed to ionize an atom or ion in a crystal such that the electron is excited to a distance r . On the other hand, the E_I is for taking that particular electron to $r \rightarrow \infty$ with $V(x) = 0$. The constant of proportionality, α is a function of averaged $V(x)$ and varies with different background atoms. For example, in $\text{La}_{1-x}\text{Ca}_x\text{MnO}_3$ system, $\text{La}_{1-x}\text{MnO}_3$ defines the background for Ca ions. Equation (26) enables one to predict quantitatively the variation of electronic properties of magnetic semiconductors with substitution. However, the quantity E_I^{real} being unknown and using E_I instead from Eq. (25) gives the nature of approximation in *iFDS* theory. Such approximation gave remarkable predictions on the evolution of $\rho(T)$ and dielectric constant with doping in high- T_c superconductors and ferroelectrics, respectively.^{11,12,16,17} One needs to employ the experimental data to determine the magnitude of $\xi = E_I^{real} = E_I + V(x)$. α in its simplest form is given by $\alpha = 1 + \frac{\langle V(x) \rangle}{E_I}$, where $\langle V(x) \rangle$ is the averaged potential. In fact, Eq. (26) suggests that even if E_I^{real} at finite r and/or $V(x)$ are not known, one can still calculate E_I for $r \rightarrow \infty$ and $V(x) = 0$, in order to predict the resistivity versus temperature curves approximately. In general, i) if $V(x) = 0$, $E_g = 0$ and $E_I \neq 0$, then we arrives at Fermi gas above E_F , ii) if $V(x) \neq 0$, $E_g = 0$ and $E_I \neq 0$, then we arrives at Fermi liquid above E_F , iii) if $V(x) \neq 0$, $E_g \neq 0$ and $E_I \neq 0$, then we arrives at Fermi liquid above E_g and iv) if $V(x) = 0$, $E_g \neq 0$ and $E_I \neq 0$, then we arrives at Fermi gas above E_g .

E. *iFDS* and its distribution functions

Both FDS and *iFDS* are for the half-integral spin particles such as electrons and holes. Its total wave function, Ψ has to be antisymmetric in order to satisfy quantum-mechanical symmetry requirement. Under such condition, interchange of any 2 particles (A and B) of different states, ψ_i and ψ_j ($j \neq i$) will result in change of sign, hence the wave function for Fermions is in the form of

$$\Psi_{i,j}(C_A, C_B) = \psi_i(C_A)\psi_j(C_B) - \psi_i(C_B)\psi_j(C_A). \quad (27)$$

The negative sign in Eq. (27) that fulfils antisymmetric requirement is actually due to one of the eigenvalue of

exchange operator,²⁵ $\mathbf{P} = -1$. The other eigenvalue, $\mathbf{P} = +1$ is for Bosons. C_A and C_B denote all the necessary cartesian coordinates of the particles A and B respectively. Equation (27) is nothing but Pauli's exclusion principle. The one-particle energies E_1, E_2, \dots, E_m for the corresponding one-particle quantum states q_1, q_2, \dots, q_m can be rewritten as $(E_{is} \pm E_I)_1, (E_{is} \pm E_I)_2, \dots, (E_{is} \pm E_I)_m$. Note here that $E_{is} = E_{initial\ state}$. It is also important to realize that $E_{is} + E_I = E_{electrons}$ and $E_{is} - E_I = E_{holes}$. Subsequently, the latter $(E_{is} \pm E_I)_i$ version where $i = 1, 2, \dots, m$ with E_I as an additional inclusion will be used to derive iFDS and its Lagrange multipliers. Denoting n as the total number of particles with n_1 particles with energy $(E_{is} \pm E_I)_1$, n_2 particles with energy $(E_{is} \pm E_I)_2$ and so on implies that $n = n_1 + n_2 + \dots + n_m$. As a consequence, the number of ways for q_1 quantum states to be arranged among n_1 particles is given as

$$P(n_1, q_1) = \frac{q_1!}{n_1!(q_1 - n_1)!}. \quad (28)$$

Now it is easy to enumerate the total number of ways for q quantum states ($q = q_1 + q_2 + \dots + q_m$) to be arranged among n particles, which is

$$P(n, q) = \prod_{i=1}^{\infty} \frac{q_i!}{n_i!(q_i - n_i)!}. \quad (29)$$

The most probable configuration at certain T can be obtained by maximizing $P(n, q)$ subject to the restrictive conditions

$$\sum_i n_i = n, \sum_i dn_i = 0. \quad (30)$$

$$\sum_i (E_{is} \pm E_I)_i n_i = E, \sum_i (E_{is} \pm E_I)_i dn_i = 0. \quad (31)$$

The method of Lagrange multipliers²⁵ can be employed to maximize Eq. (31). Hence, a new function, $F(x_1, x_2, \dots, \mu, \lambda, \dots) = f + \mu f_1 + \lambda f_2 + \dots$ is introduced and all its derivatives are set to zero

$$\frac{\partial F}{\partial x_n} = 0; \quad \frac{\partial F}{\partial \mu} = 0; \quad \frac{\partial F}{\partial \lambda} = 0. \quad (32)$$

As such, one can let the new function in the form of

$$F = \ln P + \mu \sum_i dn_i + \lambda \sum_i (E_{is} \pm E_I)_i dn_i. \quad (33)$$

After applying Stirling's approximation, $\partial F / \partial n_i$ can be written as

$$\begin{aligned} \frac{\partial F}{\partial n_i} &= \ln(q_i - n_i) - \ln n_i + \mu + \lambda(E_{is} \pm E_I)_i \\ &= 0. \end{aligned} \quad (34)$$

Thus, the Fermi-Dirac statistics based on ionization energy is simply given by

$$\frac{n_i}{q_i} = \frac{1}{\exp[\mu + \lambda(E_{is} \pm E_I)_i] + 1}. \quad (35)$$

By utilizing Eq. (35) and taking $\exp[\mu + \lambda(E \pm E_I)] \gg 1$, one can arrive at the probability function for electrons in an explicit form as

$$f_e(\mathbf{k}_{is}) = \exp \left[-\mu - \lambda \left(\frac{\hbar^2 \mathbf{k}_{is}^2}{2m} + E_I \right) \right], \quad (36)$$

Similarly, the probability function for the holes is given by

$$f_h(\mathbf{k}_{is}) = \exp \left[\mu + \lambda \left(\frac{\hbar^2 \mathbf{k}_{is}^2}{2m} - E_I \right) \right]. \quad (37)$$

The parameters μ and λ are the Lagrange multipliers. $\hbar = h/2\pi$, h = Planck constant and m is the charge carriers' mass. Note that E has been substituted with $\hbar^2 \mathbf{k}^2 / 2m$. In the standard FDS, Eqs. (36) and (37) are simply given by, $f_e(\mathbf{k}) = \exp[-\mu - \lambda(\hbar^2 \mathbf{k}^2 / 2m)]$ and $f_h(\mathbf{k}) = \exp[\mu + \lambda(\hbar^2 \mathbf{k}^2 / 2m)]$. Equation (30) can be rewritten by employing the 3D density of states' (DOS) derivative, $dn = V \mathbf{k}_{is}^2 d\mathbf{k}_{is} / 2\pi^2$, Eqs. (36) and (37), that eventually give

$$\begin{aligned} n &= \frac{V}{2\pi^2} e^{-\mu} \int_0^{\infty} \mathbf{k}^2 \exp \left[-\lambda \frac{\hbar^2 \mathbf{k}^2}{2m} \right] d\mathbf{k} \\ &= \frac{V}{2\pi^2} e^{-\mu} \int_0^{\infty} \mathbf{k}_{is}^2 \exp \left[-\lambda \frac{\hbar^2 \mathbf{k}_{is}^2}{2m} - \lambda \frac{\hbar^2 \mathbf{k}_I^2}{2m} \right] d\mathbf{k}_{is} \\ &= \frac{V}{2\pi^2} e^{-\mu - \lambda E_I} \int_0^{\infty} \mathbf{k}_{is}^2 \exp \left[-\lambda \frac{\hbar^2 \mathbf{k}_{is}^2}{2m} \right] d\mathbf{k}_{is}, \end{aligned} \quad (38)$$

$$p = \frac{V}{2\pi^2} e^{\mu - \lambda E_I} \int_{-\infty}^0 \mathbf{k}_{is}^2 \exp \left[\lambda \frac{\hbar^2 \mathbf{k}_{is}^2}{2m} \right] d\mathbf{k}_{is}. \quad (39)$$

The respective solutions for Eqs. (38) and (39) are

$$\mu + \lambda E_I = -\ln \left[\frac{n}{V} \left(\frac{2\pi\lambda\hbar^2}{m} \right)^{3/2} \right], \quad (40)$$

$$\mu - \lambda E_I = \ln \left[\frac{p}{V} \left(\frac{2\pi\lambda\hbar^2}{m} \right)^{3/2} \right]. \quad (41)$$

Note that Eqs. (40) and (41) simply imply that $\mu_e(iFDS) = \mu(T=0) + \lambda E_I$ and $\mu_h(iFDS) = \mu(T=0) - \lambda E_I$. In fact, $\mu(FDS)$ need to be varied accordingly with doping, on the other hand, *iFDS* captures the same variation due to doping with λE_I in which, $\mu(T=0)$ is fixed to be a constant (independent of T and doping). Furthermore, using Eq. (31), one can obtain

$$\begin{aligned} E &= \frac{V\hbar^2}{4m\pi^2} e^{-\mu(FDS)} \int_0^\infty \mathbf{k}^4 \exp \left[-\lambda \frac{\hbar^2 \mathbf{k}^2}{2m} \right] d\mathbf{k} \\ &= \frac{V\hbar^2}{4m\pi^2} e^{-\mu(T=0)} \int_0^\infty \mathbf{k}_{is}^4 \exp \left[-\lambda \frac{\hbar^2 \mathbf{k}_{is}^2}{2m} - \lambda \frac{\hbar^2 \mathbf{k}_I^2}{2m} \right] d\mathbf{k}_{is} \\ &= \frac{V\hbar^2}{4m\pi^2} e^{-\mu(T=0)-\lambda E_I} \int_0^\infty \mathbf{k}_{is}^4 \exp \left[-\lambda \frac{\hbar^2 \mathbf{k}_{is}^2}{2m} \right] d\mathbf{k}_{is} \\ &= \frac{3V}{2\lambda} e^{-\mu(T=0)-\lambda E_I} \left[\frac{m}{2\pi\lambda\hbar^2} \right]^{3/2} \quad (42) \\ &= \frac{3V}{2\lambda} e^{-\mu(FDS)} \left[\frac{m}{2\pi\lambda\hbar^2} \right]^{3/2}. \quad (43) \end{aligned}$$

Again, Eq. (42) being equal to Eq. (43) enable one to surmise that the total energy considered in FDS and *iFDS* is exactly the same. Quantitative comparison between Eq. (43) and with the energy of a 3D ideal gas, $E = 3nk_B T/2$, after substituting Eq. (40) into Eq. (42) will enable one to determine $\lambda = 1/k_B T$.

V. CONCLUSIONS

In conclusion, the transport properties of $\text{Ga}_{1-x}\text{Mn}_x\text{As}$, $\text{La}_{1-x}\text{Ca}_x\text{MnO}_3$ and $\text{Mn}_x\text{Ge}_{1-x}$ can be characterized with a model consists of ionization energy based Fermi-Dirac statistics coupled with spin disorder scattering mechanism. This model has been able to explain the evolution of resistivity's curves with respect to temperature and Mn doping. The arguments for the incompatibility between the calculated and experimentally determined normalized magnetization is based on the total current's tendency to obey the principle of least action. The validity of $E_I + E_F$ and $M_\rho(T, M_0)$ have been justified quantitatively by computing p and $M_\rho(T)/M_0$ respectively, which are in excellent agreement with the experimental results. However, the magnitudes of A and B are not diagnosed due to unknown reliable values of A_h , J_{ex} and E_F . To

this end, the variation of hole mobilities and dielectric constant with doping, the influence of multiple exchange

FIG. 1: Equation (7) has been employed to fit the experimental $\rho(T)$ plots for $\text{Ga}_{1-x}\text{Mn}_x\text{As}$ as given in a) whereas Eq. (9) is used to fit the plots in b). All fittings are indicated with solid lines. b) is actually for annealed non-ferromagnetic $\text{Ga}_{0.930}\text{Mn}_{0.070}\text{As}$ samples. c) and d) show the T variation of calculated $M_\alpha(T)/M_{4.2}$ ($\alpha = \text{K}, \text{TD}, \rho$) with $S = 1$ for $x = 0.060$ and 0.070 respectively. $M_K(T)/M_{4.2}$ is also calculated with $S = 5/2$. The experimental $M_{exp}(T)/M_{4.2}$ plot for $x = 0.070$ (as grown) is shown in d).

FIG. 2: Experimental plots of $\rho(T)$ for $\text{La}_{1-x}\text{Ca}_x\text{MnO}_3$ at $x = 0.1, 0.2$ and 0.2 (6 T) have been fitted with Eq. (6) as depicted in a) and b). All fittings are indicated with solid lines. Whereas c) and d) show the T variation of calculated $M_\alpha(T)/M_{4.2}$ ($\alpha = \text{K}, \rho$) with $S = 1$ for $x = 0.1$ and 0.2 respectively. The experimental $M_{exp}(T)/M_{4.2}$ plot for $x = 0.2$ is given in d).

interaction and energy gap above T_C should be investigated experimentally. We have also justified the application of *iFDS* based resistivity model by showing the *iFDS* wave functions are exactly the same with the wave functions obtained from the ladder-operator and recursion-formula methods.

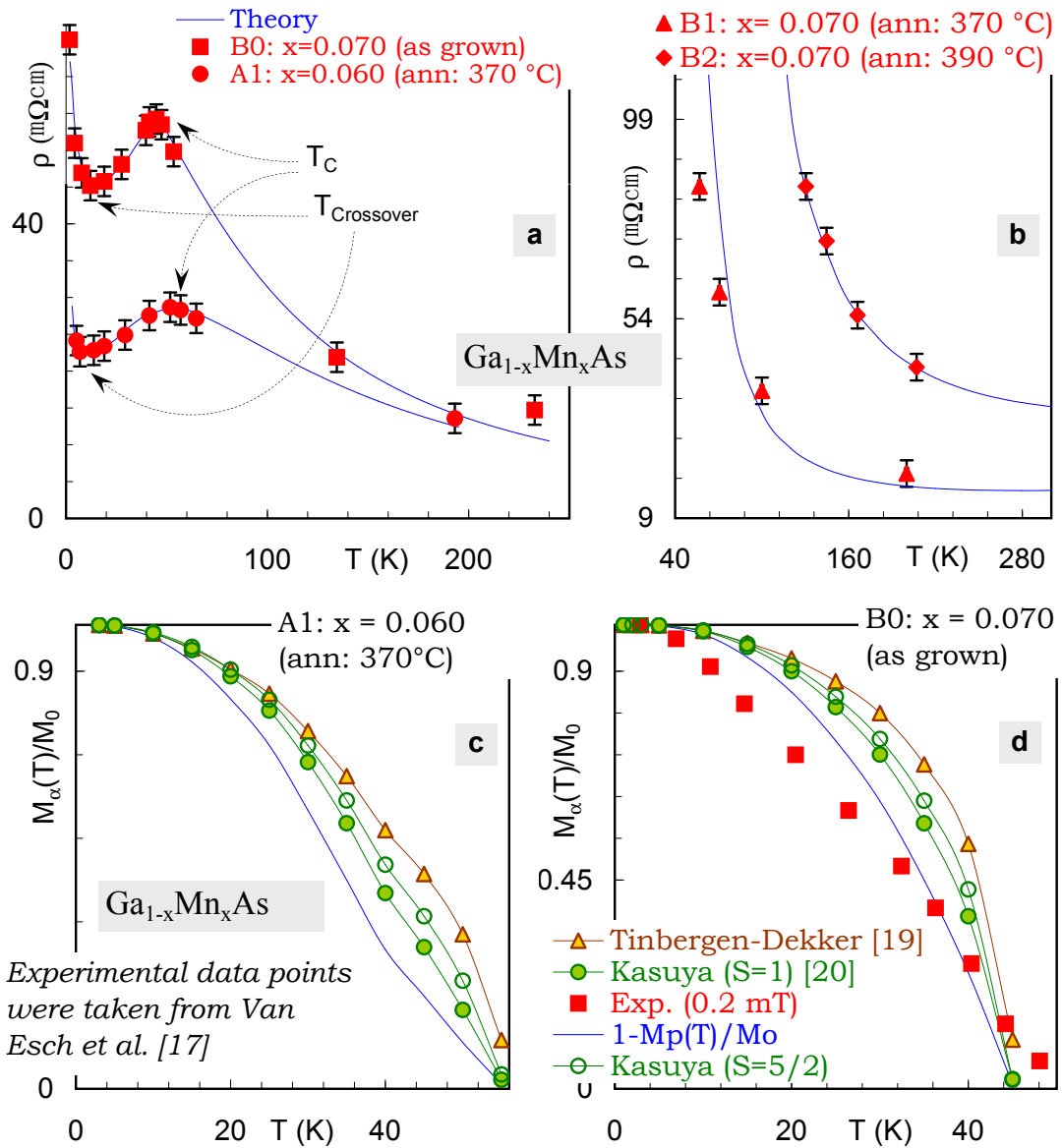
Acknowledgments

The author is grateful and beholden to Arulsamy Innasimuthu, Sebastiammal Innasimuthu, Arokia Das Anthony and Cecily Arokiam of CMG-A for their unconditional financial support. ADA also thanks Bryne J.-Y. Tan, Jasper L. S. Loverio and Hendry Izaac Elim for their kind help with figure preparations and references.

FIG. 3: a) Equation (7) has been employed to fit the experimental $\rho(T)$ plots for $\text{Mn}_{0.02}\text{Ge}_{0.98}$. The plot with additional constraint, $dM_\rho(T)/dT = 0$ on Eq. (7) is also given to emphasize the influence of $M_\rho(T)/M_0$ for an accurate fitting. In these two plots, $A = 25$, $B = 1060$ and $E_I + E_F = 15$ K. The T -dependence of $\rho(T)$ in accordance with J_e only, ignoring J_{se} is calculated with Eq. (9), which lacks the ability to capture the experimental $\rho(T, x = 0.02)$. In this case, $A_h = 1.8$ and $E_I + E_F = 15$ K. Both $E_I + E_F = 15$ K and $E_I + E_F = 80$ K give p in the order of 10^{19} cm^{-3} using Eq. (6) and $m_h^* = \text{rest mass}$. b) Shows the T variation of $M_\alpha(T)/M_0$ ($\alpha = \text{K}, \rho, exp$) for $x = 0.02$. Notice the inequality, $M_K(T)/M_0 > M_\rho(T)/M_0 > M_{exp}(T)/M_0$ that arises as a result of the principle of least action. The T -dependence of $M_\alpha(T)/M_0$ is close to the $\text{Ga}_{1-x}\text{Mn}_x\text{As}$ DMS, rather than the traditional manganites. As such, this behavior is suspected to be associated with the multiple exchange interaction.

TABLE I: Calculated values of T independent electron-electron scattering rate constant (A), B , which is a function of T independent spin disorder scattering rate constant and spin exchange energy (J_{ex}) as well as the ionization energy (E_I). All these parameters are for Mn doped $\text{Ga}_{1-x}\text{Mn}_x\text{As}$ (as grown and annealed at 370 °C, 390 °C) and Ca doped $\text{La}_{1-x}\text{Ca}_x\text{MnO}_3$ (measured at 0 and 6 T) systems. All $\text{Ga}_{1-x}\text{Mn}_x\text{As}$ samples were measured at 0 T.

-
- ¹ R. Horyn, A. Sikora, E. Bukowska, *Physica C* **387**, 277 (2003).
- ² N. Chan, P. Q. Niem, H. N. Nhat, N. H. Luong, N. D. Tho, *Physica B* **327**, 241 (2003).
- ³ R. Demin, Koroleva, R. Szymczak, H. Szymczak, *Phys. Lett. A* **296**, 139 (2002).
- ⁴ A. Van Esch, L. Van Bockstal, J. De Boeck, G. Verbanck, A. S. van Steenbergen, P. J. Wellmann, B. Grietens, R. Bogaerts, F. Herlach, G. Borghs, *Phys. Rev. B* **56**, 13103 (1997).
- ⁵ R. Mahendiran, S. K. Tiwary, A. K. Raychaudhuri, T. V. Ramakrishnan, R. Mahesh, N. Rangavittal, C. N. R. Rao, *Phys. Rev. B* **53**, 3348 (1996).
- ⁶ Tineke Van Peski-Tinbergen, A. J. Dekker, *Physica* **29** 917 (1963).
- ⁷ T. Kasuya, *Prog. Theor. Phys.* **16**, 58 (1956).
- ⁸ H. Ohno, *Science* **281**, 951 (1998).
- ⁹ Y. D. Park, A. T. Hanbicki, S. C. Erwin, C. S. Hellberg, J. M. Sullivan, J. E. Matson, T. F. Ambrose, A. Wilson, G. Spanos, B. T. Jonker, *Science* **295**, 651 (2002).
- ¹⁰ A. Das Arulsamy, cond-mat/0212202 (Unpublished).
- ¹¹ A. Das Arulsamy, *Physica C* **356**, 62 (2001).
- ¹² A. Das Arulsamy, *Phys. Lett. A* **300**, 691 (2002).
- ¹³ A. Das Arulsamy, P. C. Ong, M. T. Ong, *Physica B* **325**, 164 (2003).
- ¹⁴ A. Das Arulsamy, *Physica B* **352**, 285 (2004).
- ¹⁵ A. Das Arulsamy, *Physica C* **420**, 95 (2005).
- ¹⁶ A. Das Arulsamy, in: Paul S. Lewis (Ed.), *Superconductivity Research at the Leading Edge*, Nova Science Publishers, New York, 2004, pp. 45-57; A. Das Arulsamy, cond-mat/0408613.
- ¹⁷ A. Das Arulsamy, *Phys. Lett. A* **334**, 413 (2005).
- ¹⁸ J. J. Tu, G. L. Carr, V. Perebeinos, C. C. Homes, M. Strongin, P. B. Allen, W. N. Kang, E. -M. Choi, H. -J. Kim, S. -I. Lee, *Phys. Rev. Lett.* **87**, 277001 (2001).
- ¹⁹ N. Mannella, A. Rosenhahn, C. H. Booth, S. Marchesini, B. S. Mun, S. -H. Yang, K. Ibrahim, Y. Tomioka, and C. S. Fadley, *Phys. Rev. Lett.* **92**, 166401 (2004).
- ²⁰ A. Banerjee, B. K. Chaudhuri, A. Sarkar, D. Sanyal, D. Banerjee, *Physica B* **299**, 130 (2001).
- ²¹ A. Banerjee, S. Pal, B. K. Chaudhuri, *J. Chem. Phys.* **115**, 1550 (2001).
- ²² L. Van Bockstal, A. Van Esch, R. Bogaerts, F. Herlach, A. S. van Steenbergen, J. De Boeck, G. Borghs, *Physica B* **246-247**, 258 (1998).
- ²³ K. Ando, T. Hayashi, M. Tanaka, A. Twardowski, *J. Appl. Phys.* **53**, 6548 (1998).
- ²⁴ M. J. Winter (<http://www.webelements.com>).
- ²⁵ D. J. Griffiths, *Introduction to Quantum Mechanics*, Prentice-Hall, New Jersey, 1995.



Sample	Ann. $T(\textcolor{red}{H})$ °C(Tesla)	A [Calc.]	B [Calc.]	$E_I + E_F$ [Calc.] K(meV)	$T_C(\textcolor{red}{T}_{cr})$ K [17,18]
$\text{Ga}_{0.940}\text{Mn}_{0.060}\text{As}$ [1]	370 (0)	4.5	400	8 (0.69)	50 (10)
$\text{Ga}_{0.930}\text{Mn}_{0.070}\text{As}$ [1]	As grown (0)	9.2	400	12 (1.04)	45 (12)
$\text{Ga}_{0.930}\text{Mn}_{0.070}\text{As}$ [1]	370 (0)	0.02	~	280 (24.2)	~
$\text{Ga}_{0.930}\text{Mn}_{0.070}\text{As}$ [1]	390 (0)	0.03	~	400 (34.5)	~
$\text{La}_{0.9}\text{Ca}_{0.1}\text{MnO}_3$ [2]	~ (0)	10	0.65	1400 (121)	222 (~)
$\text{La}_{0.8}\text{Ca}_{0.2}\text{MnO}_3$ [2]	~ (0)	10	1.2	1300 (112)	246 (~)
$\text{La}_{0.8}\text{Ca}_{0.2}\text{MnO}_3$ [2]	~ (6)	5	3.2	900 (78)	251 (~)

